Hierarchical imaging of the human knee

Georg Schulz[a], Christian Götz[a], Hans Deyhle[a], Magdalena Müller-Gerbl[b], Irene Zanette[c],
Marie-Christine Zdora[c], Anna Khimchenko[a], Peter Thalmann[a],
Alexander Rack[d] and Bert Müller[a]

[a]Biomaterials Science Center, Department of Biomedical Enginnering, University of Basel,
Switzerland;
[b]Musculoskeletal Research, Department of Biomedicine, University of Basel, Switzerland;
[c]Diamond Light Source, Harwell Science & Innovation Campus, Didcot, United Kingdom;
[d]European Synchrotron Radiation Facility, Grenoble, France

ABSTRACT

Among the clinically relevant imaging techniques, computed tomography reaches the best spatial resolution. Sub-millimeter voxel sizes are regularly obtained. For investigations on true micrometer level lab-based micro-tomography μCT has become gold standard. The aim of the present study is the hierarchical investigation of a human knee post mortem using hard X-ray μCT. After the visualization of the entire knee using a clinical CT with a spatial resolution on the sub-millimeter range, a hierarchical imaging study was performed using the laboratory μCT system nanotom® m. Due to the size of the whole knee the pixel length could not be reduced below 65 μm. These first two data sets were directly compared after a rigid registration using a cross-correlation algorithm. The μCT data set allowed an investigation of the trabecular structures of the bones. The further reduction of the pixel length down to 25 μm could be achieved by removing the skin and soft tissues and measuring the tibia and the femur separately. True micrometer resolution could be achieved after extracting cylinders of several millimeters in diameter from the two bones. The high resolution scans revealed the mineralized cartilage zone including the tide mark line as well as individual calcified chondrocytes. The visualization of soft tissues including cartilage, was arranged by X-ray grating interferometry at ESRF and Diamond Light Source. Whereas the high-energy measurements at ESRF allowed the simultaneous visualization of soft and hard tissues, the low-energy results from Diamond Light Source made individual chondrocytes within the cartilage visible.

Keywords: Microtomography, laboratory X-ray source, human knee, cartilage, X-ray phase contrast, grating interferometry

1. INTRODUCTION

The human musculoskeletal system generally works for decades. It consists of a variety of hard and soft tissue components. Even the hard tissue components are not static but change their morphology, termed bone remodeling, owing to the metabolism. This lifelong process includes the removal of mature bone tissue from the skeleton, termed bone resorption, and the formation of new bony tissues. In adults, it was found that about 10% of the bone is remodeled per year [1]. Bone remodeling is essential to repair all kind of fractures, which even occur during daily activity. Diseases such as osteoporosis are caused by the imbalance of bone resorption and bone formation and therefore reflect the structural changes on the macroscopic and microscopic levels. The micro- and macroanatomy of the human joints, therefore, characterizes the state of health, which correlates with physical activity, sex, and age. The investigation of joints such as the knee belongs therefore to the daily business in radiology. Whereas clinical computed tomography (CT) reveals the bony tissue with a spatial resolution down to a fraction of a millimeter, magnetic resonance imaging (MRI) exhibits data of inferior resolution than CT, but is applied to visualize the soft tissue components because of superior contrast. The microanatomy, however, is not accessible using the radiological means. In some cases, bone biopsies were used to determine the microstructure of bone, the related severity of osteoporosis, and the related mechanical properties of bone by means of μCT

Further author information: (Send correspondence to G.S.) E-mail: georg.schulz@unibas.ch, Telephone: +41 61 265 9125, Fax: +41 61 265 9699; www.bmc.unibas.ch

[2–4]. Post mortem studies even allow three-dimensionally evaluating the ultra-structure of bone, see e.g. Peyrin et al. [5]. The studies mentioned above, however, concentrate on the hard tissues. The simultaneous visualization of soft and hard tissue components using micro computed tomography (μCT) is challenging, since the X-ray attenuation of soft and hard tissue significantly differs [6]. For an optimized choice of the photon energy, the cartilage, for example, is almost fully transparent, whereas the bone shows the streak artifacts characteristic for photon energies, which are too low. In such cases, the use of phase tomography is of advantage [7].

The present study covers the full range of length scales from the entire knee down to individual chondrocytes. For this purpose, the authors used a conventional CT, as currently available at radiology departments, an advanced conventional μCT system, as available at the Biomaterials Science Center in Basel, and the synchrotron radiation facilities at ESRF and Diamond in absorption and phase contrast modes. The goal of this study is to demonstrate the performance of these CT systems in the morphological characterization of a human knee. The registration of the tomography data [8] enables a direct comparison between the modalities for the selected human knee and its parts. The results allow for the proper choice of modality to characterize any other joint from mammalians on the desired length scale down to the cellular level.

2. MATERIALS AND METHODS

2.1 Specimen preparation

Within 24 hours of death the knee of an 87 years old female was fixed in 10% formalin following the standard protocol of the Institute of Anatomy at the University of Basel. After fixation, the knee was extracted by transversal cuts about 10 cm above and below the femorotibial joint space. At this point, absorption based medical CT and laboratory μCT scans were acquired. For these two scans, the knee was taken out of the formalin-solution and measured in air. To prevent the tissue from drying out, the sample was then stored in a 4% formalin solution. During all further scans, the samples were kept in the container with the formalin.

After the first two scans the skin, fat and muscle tissues were removed. Absorption contrast based μCT scans of the separated femur and tibia were performed with the nanotom® m. For further observations, regions of interest (ROI) had to be determined where cylinders were extracted by drilling or using a metal hollow punch. The examination by eye showed that the cartilage cover was, except for some areas of the femoropatellar joint, in good shape, considering the age of the donor. The ROI on the femur (see Fig. 1) was selected around the contact area of the femorotibial joint where a relatively thick cartilage layer was preserved. This region is exposed to high mechanical loadings and can therefore be expected to show increased mineralization in the subchondral plate [9]. The area around the proximal end of the anterior cruciate ligament (ACL) on the tibia was selected to be the ROI of choice within the tibial plateau. This region was seen to be the only one where a sample consisting of not only bone and cartilage but also ligament tissue could be taken. Femoral and tibial cylinders were extracted from 1-2 cm sections (Fig. 1) for further higher resolved measurements with the nanotom® m and at the synchrotron radiation facilities. The small cylinders were stored in Eppendorfer containers, the larger
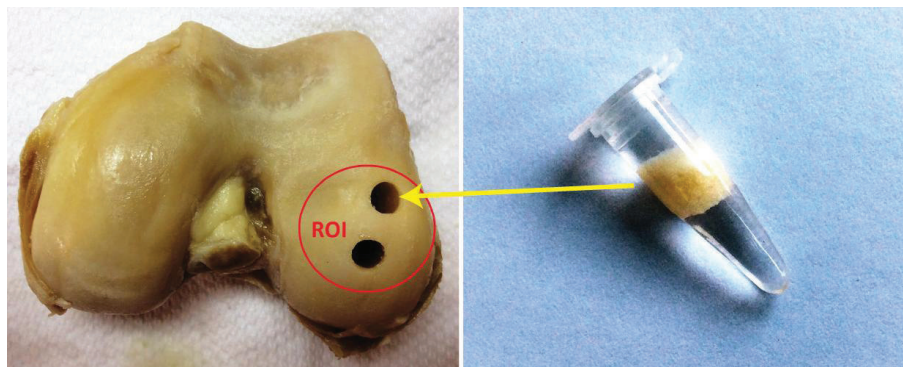

Figure 1. Selected ROI of femoral slice where two cylinders were extracted. The extracted specimen was transferred in an Eppendorfer container filled with formalin.

Table 1. Parameters of microtomography scans. Specimen: Tib. cyl.: tibial cylinder, Fem. cyl.: femoral cylinder; Facility: medCT: medical CT scanner Siemens Somatom Emotion 16; Method: AC: absorption contrast, GI: grating interferometry; U: acceleration voltage; E: photon energy; I: beam current; Proj.: number of projections over 360°; Exp.: exposure time.

Scan #	Specimen	Facility	Method	Voxel [μm]	U [kV]	E [keV]	I [mA]	Proj.	Exp. [s]
1	Entire knee	medCT	AC	300.0*	130		25.00	1250	15.0**
2	Entire knee	nanotom	AC	65.0	180		0.03	2000	6.0
3	Femur	nanotom	AC	25.0	150		0.05	3000	8.0
4	Tibia	nanotom	AC	25.0	150		0.05	3000	8.0
5	Tib. cyl.	nanotom	AC	8.0	60		0.31	1600	3.0
6	Tib. cyl.	ESRF	GI	5.1		52		1600	0.5***
7	Fem. cyl.	nanotom	AC	3.0	40		0.35	2000	6.0
8	Fem. cyl.	Diamond	GI	2.3		19		1600	5.0***

*In-plane pixel length, slice thickness: 600.0 μm.
**Whole scan time.
***Exposure time per phase step image.

ones in closed plastic tubes, all filled with 4% formalin solution. The exact diameters of the extracted cylinders were determined by the detector pixel length. They measured 5 mm for the femoral plug scanned at Diamond and 10 mm for the tibial plug measured at the ESRF.

2.2 Medical CT

The medical scan (Table 1, scan number 1) was acquired using a Siemens Somatom Emotion® 16 medical CT scanner. The reconstructed data set had an anisotropic voxel size of $0.3 \times 0.3 \times 0.6 \ mm^3$. A smooth reconstruction kernel (B31s) was chosen to show favorable contrast for soft tissues.

2.3 X-ray microtomography

After medical CT scans all samples from entire knee down to the few millimeters sized cylinders, were measured using the nanotom® m (phoenix|x-ray, GE Sensing & Inspection Technologies GmbH, Wunstorf, Germany). The selected parameters are shown in Table 1 (scan numbers 2-5 and 7). The parameters were chosen depending on the sizes of the specimens. The whole scan times varied between 80 min for the extracted cylinders and almost 17 h for the entire knee measurements. For the nanotom® m measurements of the larger parts (entire knee, femur, tibia) an additional 0.3 mm Cu filter was mounted between source and specimen in order to reduce beam hardening.

2.4 X-ray grating interferometry

The experiments at ESRF (Grenoble, France) were performed at the beamline ID19 (Table 1, scan number 6) where the photon energy was set to 52 keV in order to visualize hard and soft tissues simultaneously [7]. The beam-splitter grating g_1 had a periodicity of $p_1 = 4.785 \ \mu m$ and a Si structure height of 9.2 μm and the analyzer grating g_2 a periodicity of $p_2 = 2.400 \ \mu m$ and a Au structure height of 100 μm. The ratio of the grating periods, p_2/p_1, was matched to the beam divergence with a distance between source and interferometer of 150 m and a distance between the gratings of $d = 480 \ mm$ (corresponding to the 1st Talbot order) [10]. The container containing the tibial cylinder in formalin solution was fixed at the high precision rotation stage and immersed in a water-filled tank with parallel polymethylmethacrylat plates. The detectors CCD is of size 2048×2048 pixels. Over 360° 1600 projections were recorded (e.g. step size of 0.225°). Four phase-stepping images were taken at each projection angle with an exposure time of 0.5 s each.

The cylindrical femoral specimen was measured at I13-2 (Diamond Light Source, Harwell, UK), the parameters are shown in Table 1, scan number 8. The photon energy was set to 19 keV in order to be sensitive enough to
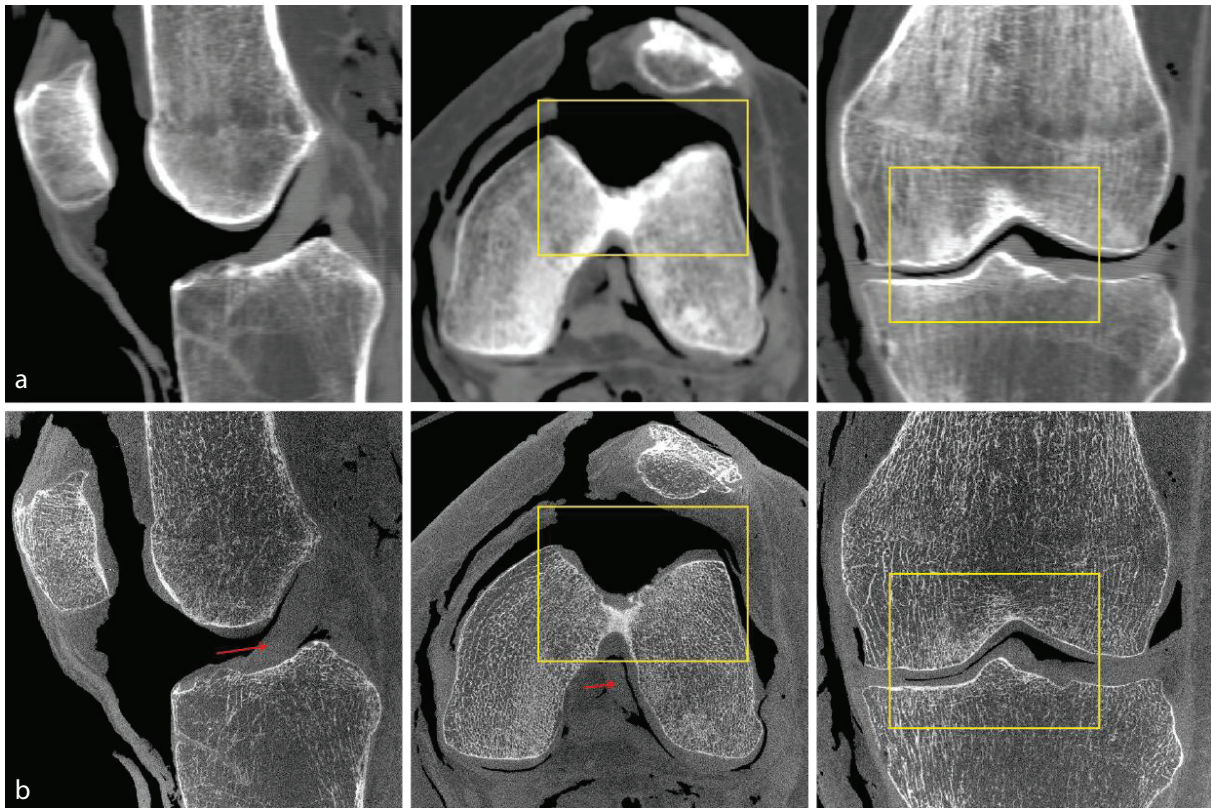
Figure 2. Corresponding sagittal, transversal and frontal slices of the entire knee joint (left knee). Medical CT (a) is compared to laboratory based nanotom® m μCT (b). With comparable contrast for soft tissues, the nanotom® m data set shows improved details of the trabecular network due to its higher resolution.

visualize small electron density differences within the cartilage. The interferometer consisted of a beam-splitter grating g_1 with a periodicity of $p_1 = 4.79$ μm and a Si structure height of 23 μm and an absorption grating having a periodicity of $p_2 = 2.40$ μm and a Au structure height of 109 μm. The intergrating distance was set to 48 cm which corresponds to the 9th Talbot order. A total number of 5 phase steps were acquired at each projection angle. During the scanning procedure, the sample was again kept in a small water tank with parallel polymethylmethacrylat plates.

2.5 Data treatment

The nanotom® m radiographs were reconstructed using the software phoenix datos|x 2.0.1 - RTM (GE Sensing & Inspection Technologies GmbH, Wunstorf, Germany) where a cone beam filtered back-projection algorithm is used.

The data obtained at the synchrotron facilities (ESRF and Diamond Light Source) using XGI was phase-retrieved using pixel-wise Fourier analysis. The processed phase projections were then reconstructed using a modified filter kernel (Hilbert transform) in combination with standard filtered back-projection algorithm [11,12].

For the comparison of same regions, the different datasets were registered. A pre-registration was performed using the software VGStudio MAX 2.1 (Volume Graphics GmbH, Heidelberg, Germany). For the final registration a three-dimensional rigid algorithm with six degrees of freedom, namely three translation and three rotation degrees, was used [13]. The registration was performed using the maximization of mutual information principle [14,15]. Limitations in data size required by the registration software enforced binning of the corresponding data sets in some cases.
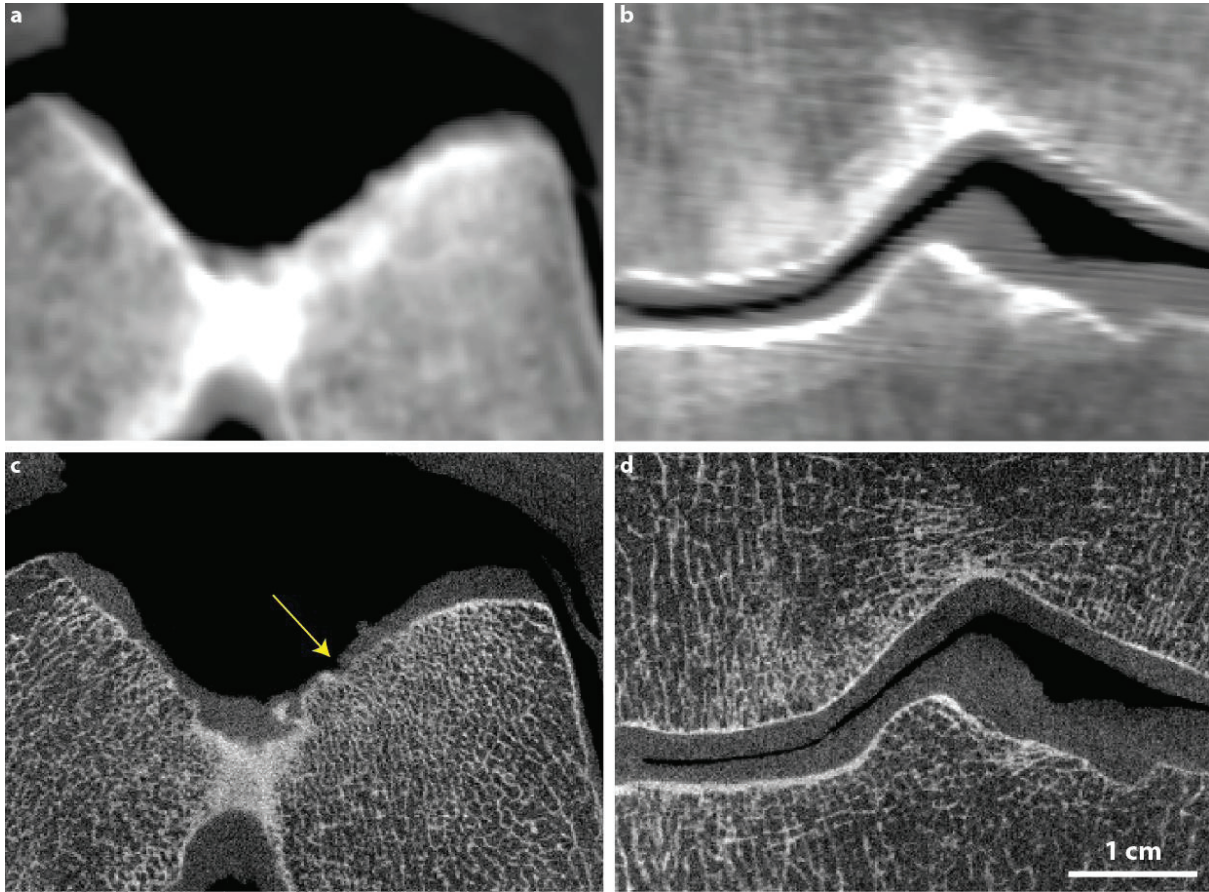
Figure 3. Magnifications from the transversal and sagittal slices of Fig. 2. The medical CT images (a, b) are compared to the nanotom® images (c, d). Yellow arrow in (c) shows regions with cartilage degeneration in detail.

3. RESULTS

3.1 Entire knee: Medical CT vs. microtomography

Before the tomography experiments, the knee was used for medical students training where it was opened. After the operation training the knee was closed again by stitching the skin. This can be seen on the back regions in the soft tissue and joint capsule in Fig. 2. The nanotom® m scan (Fig. 2, (b)) shows the trabecular structure of the bone in detail and offers sharp edges on tissue borders in comparison to the medical CT (Fig. 2, (a)). On the sagittal slices (Fig. 2, left images), all three composing bones of the knee joint (i.e. femur, tibia and patella) can be seen. The slice position was chosen between the condyles cutting through the fossa intercondylaris. The anterior cruciate ligament (ACL) can be depicted clearly in both, the sagittal and transversal sections (red arrows). The yellow rectangles in the transversal and frontal slices show the location of the magnified images (Fig. 3). The cartilage covering can be seen well in both medical CT and μCT images (Fig. 3). However the higher resolution of the μCT data allows a much clearer delineation towards the background. For regions with cartilage degeneration, it shows precise details, not only of the thinned cartilage layer but also of the underlying bone structures. This can be seen in the femoral trochlea where the subchondral bone plate is damaged in the vicinity of a cartilage defect (yellow arrow). The μCT resolution is needed in this case to make this pathologic alteration visible.

The distal end of the ACL at the area intercondylaris anterior of the tibia has almost the same gray value as the cartilage (Fig. 3, (b) and (d)). Therefore the two tissues cannot be differentiated. By comparing the μCT image (Fig. 3, (d)) with the corresponding medical CT image (Fig. 3, (b)), it can be demonstrated how the
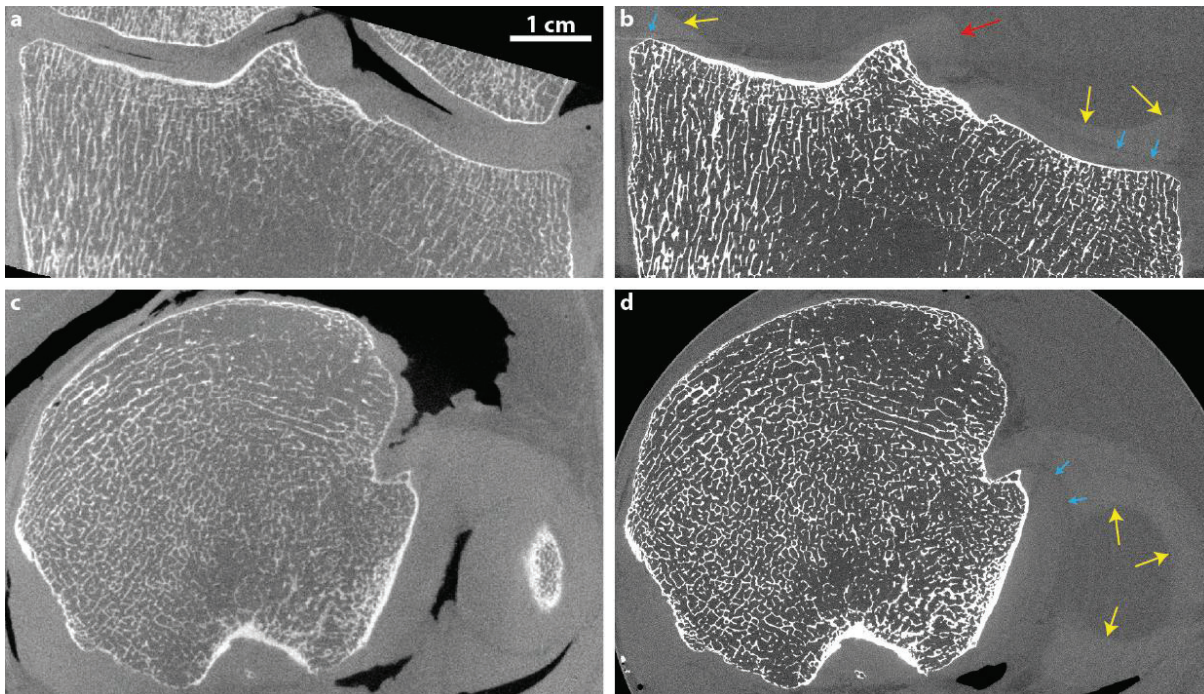
Figure 4. Frontal and transversal (tilted) slices of the tibial bone. μCT data of the extracteded tibia (b, d) was compared with the μCT of the entire knee (a, c), both scanned with nanotom® m. The arrows represent borders between soft tissues and formalin solution.

higher resolution emphasizes the trabecular network structures. The trabecular structures are aligned according to the loading forces (see Fig. 3, (d)), vertically inside the condyles and rather horizontally in between.

3.2 Microtomography of extracted tibia

The μCT data set of the extracted tibial bone stored in formalin was compared with the data set of the entire knee scanned in air presented in section 3.1. Hence the identification of soft tissues becomes more challenging. Nevertheless cartilage, menisci and cruciate ligament can be detected. The yellow colored arrows in Fig. 4, (b) and (d) show the two menisci. They are visible due to sufficient contrast compared to the surrounding formalin. This is also the case for the ACL (red arrow) and the cartilage. The latter shows comparable gray values to the menisci but can nevertheless be distinguished. The higher resolution images show a thin formalin layer between the two tissues (blue arrows). The frontal sections are chosen at the location where the ACL is attached to the tibial bone (area intercondylaris anterior).

3.3 Cellular resolution of tibial cylinder

The tibial cylinder (Table 1, scan number 5) was registered to the extracted tibia (Table 1, scan number 4). All the slices in Fig. 5 show a nearly frontal orientation. Images (a) and (c) of Fig. 5 display a view of the anterior eminentia intercondylaris which appears in the shape of a mountain. The left slope leads down to the condylus medialis and is covered by a cartilage layer. The latter can just be differentiated from the background (formalin) along its surface line (blue arrows). The higher resolution of the images (c) and (d) in Fig. 5 leads to a sharper delineation but can nevertheless not provide a better contrast for the cartilage tissue. The right slope rolls down towards the rough area intercondylaris anterior. This is where the ACL (red arrow) merges with the bone. Like the cartilage tissue, the ligament can only be hardly differentiated from the formalin background. The high resolution zoomed-in image (Fig. 5, d) offers good insights into the anatomy of the subchondral bone. At certain areas an intermediate layer between bone and cartilage is visible (magenta and white arrows). This layer is associated with the so called mineralized cartilage zone [16]. Again the white arrows show the transition from
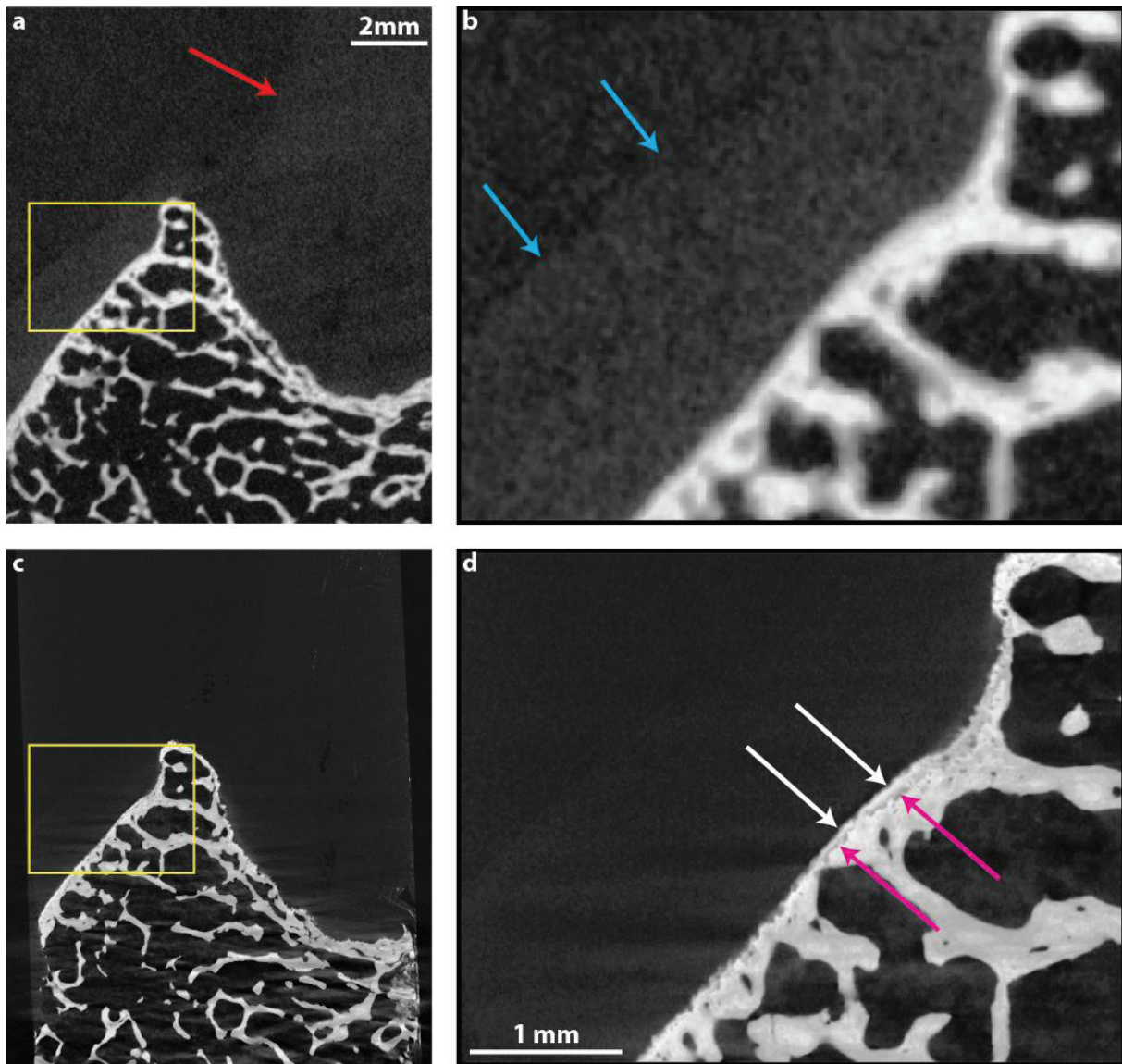
Figure 5. Zoom-in of the μ CT data of the separated tibia (a) compared to a registered slice of the extracted tibial cylinder (c) and magnified images of the yellow marked regions (b, d). Both data sets were acquired using nanotom® m. High resolution images (d) show the texture of the subchondral bone in high detail.

the cartilage and the pink arrows that from the subchondral bone to this intermediate layer. The demarcation towards the cartilage marked with the white arrows presumably represents the tide mark line. Due to their location, the bright circular structures are assumed to be calcified chondrocytes.

3.4 High-energy XGI of tibial cylinder

This section compares the absorption-based data obtained with the nanotom® m (Table 1, scan nr. 5) with the grating-based data acquired at the ESRF (Table 1, scan nr. 6). The slices are roughly taken from the same region as in 3.3 (Fig. 5). The orientation though is slightly different due to the registration process. The XGI images (Fig. 6, (b) and (d)) show a better contrast between the soft tissues (i.e. cartilage and ACL) and the formalin background. The cartilage layer can be seen clearly without showing any information about its internal structures. It appears as a homogenous tissue layer. The ACL on the other hand shows a clear texture. The
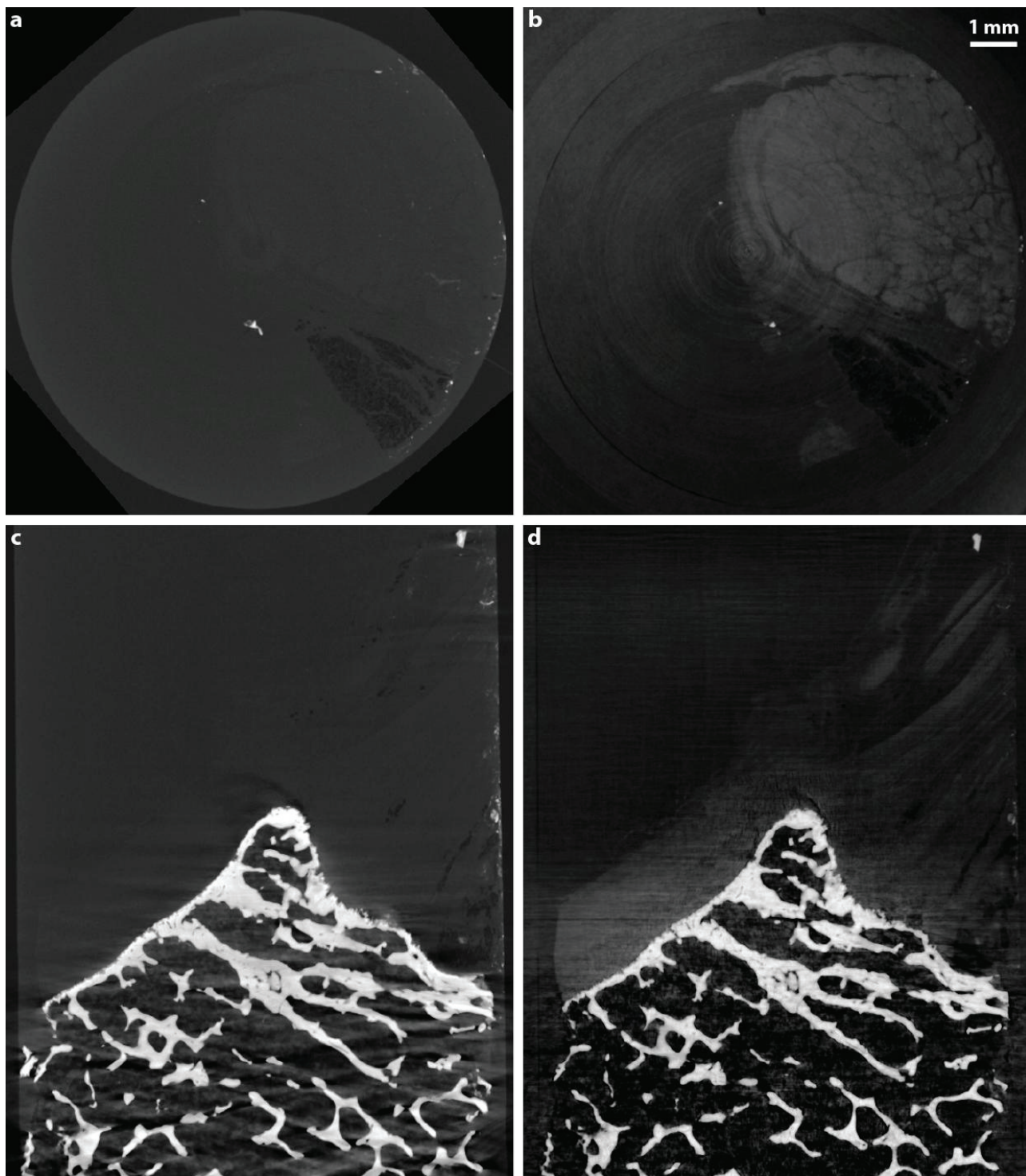
Figure 6. Selected absorption-based nanotom® m slices (a) and (c) and the corresponding XGI slices (b) and (d). Transversal (top) and frontal sections (bottom). The phase contrast data shows noticeable better contrast for soft tissues like cartilage and cruciate ligament.
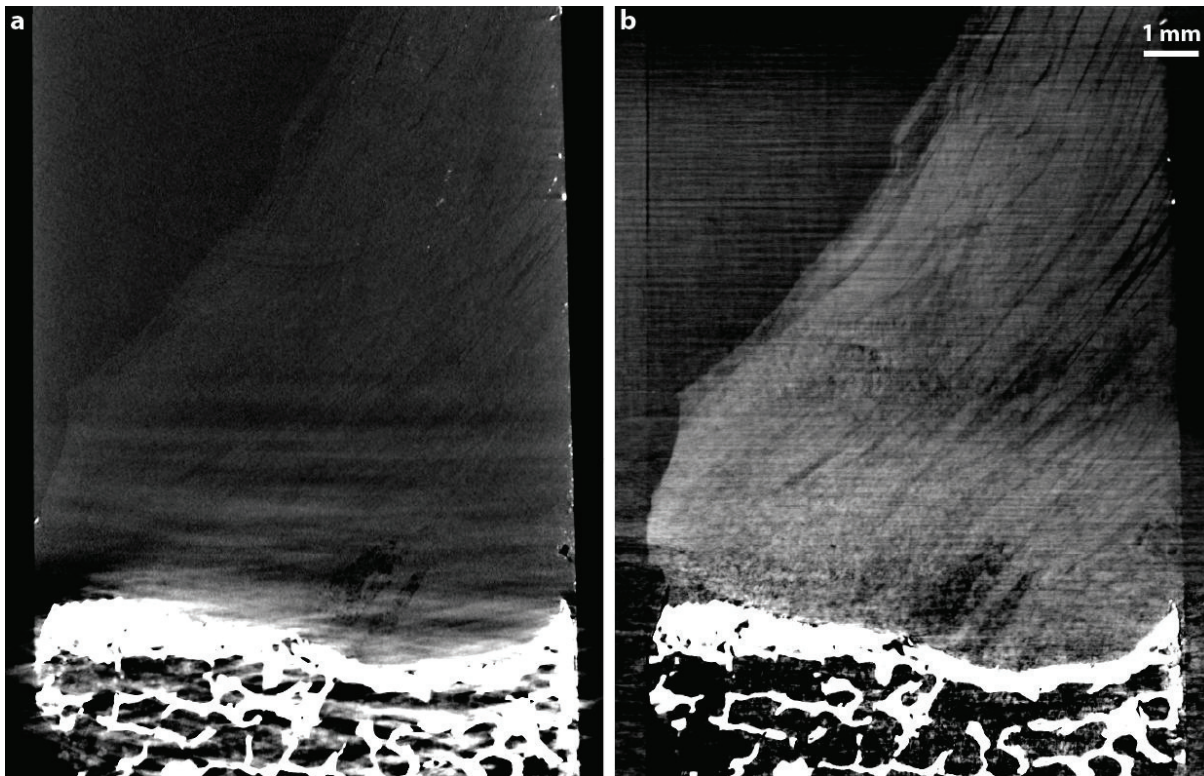
Figure 7. Nanotom®m (a) and ESRF (b) image of the ACL. The grating-based PC image obtained at ESRF shows the ligament texture in detail.

fiber bundles of the ACL have a prefered diagonal orientation in image (d) and are cut transversally in image (b) of Fig. 6.

Fig. 7 focuses on the visualization of the ACL in more detail. Due to optimization of the gray scale range for soft tissues the bone appears oversaturated. The choice of the gray scale range nevertheless shows that the nanotom® m is capable of distinguishing the ACL from the formalin solution (Fig. 7, a). Again it can be seen that XGI (Fig. 7, b) represents the fibres of the ligament in more detail. The contrast-to-noise ratios (CNR) (Table 2) give a quantitative explanation of the previously presented qualitative results. It can be seen that the CNRs of the ESRF data are slightly higher when comparing soft tissue to the background formalin. That is why cartilage and ligament can be better differentiated from the background.

3.5 Low-energy XGI of femoral cylinder

In this last section, the nanotom® m (Table 1, scan number 7) and XGI data sets (Table 1, scan number 8) of the femoral cylinder were compared. In order to have a higher sensitivity needed to visualize the smallest electron density differences within soft tissues, lower energy compared to section 3.4 was chosen. Again, the nanotom® m data set shows a superior hard tissue contrast (Fig. 8, (a)). The bone and the mineralized cartilage layer close

Table 2. CNR comparison of the tibial cylinder data acquired with the nanotom® m and at ESRF using GI.

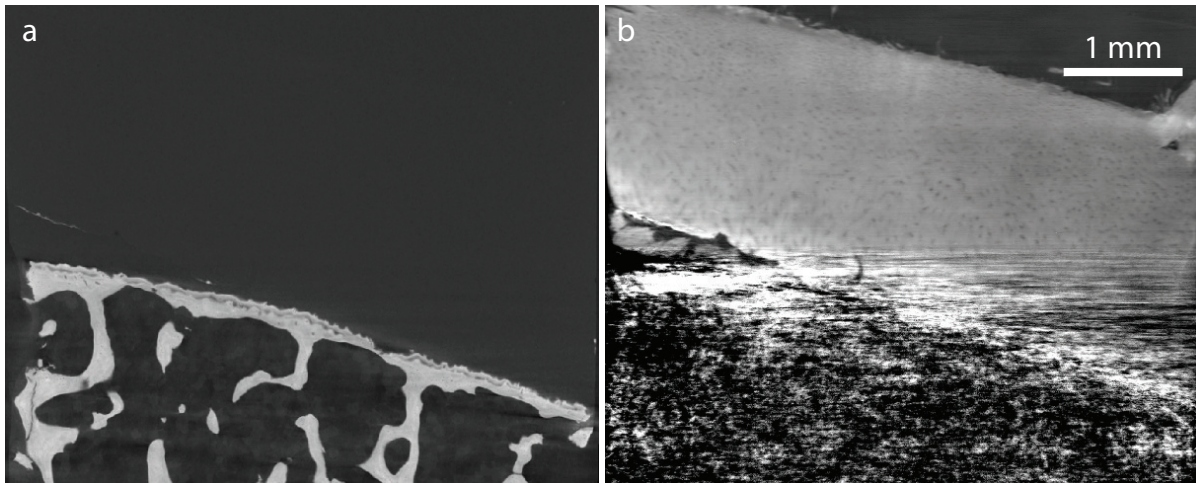| Modality	Cartilage / Formalin	ACL / Formalin
nanotom	3.8	1.1
GI @ESRF	4.1	1.5

Figure 8. Registered sections of the femoral cylinder acquired using nanotom® m (a) and XGI reconstruction (b). The phase contrast data offers superb soft tissue contrast presenting an insight into the cartilage layer.

to the subchondral bone shown in section 3.3 are not visible in the XGI data (Fig. 8, (b)). The phase contrast image shows the huge artefacts because of the low energy choice. On the other hand the internal structures of the cartilage are visible in detail. Individual chondrocytes respectively their surrounding low-density fluidic lagunae show up as black spots inside the cartilage layer. Often more than one chondrocyte are located inside the same lagunae resulting in an ellipsoidal shape. To gain more stiffness for the cartilage tissue, they show a perpendicular orientation towards the surface in the vicinity of bone. In the outer region of the cartilage (top border in the image) they are generally smaller and rather oriented parallel to the surface.

4. DISCUSSION AND CONCLUSIONS

In the first step of the study a comparison between an advanced medical CT and an advanced laboratory μCT system was performed. For the μCT images, no noise-reducing smoothing filter was applied to. This explains the salt like noise, which is much more prominent than in the medical CT (Figs. 2 and 3). The medical CT data set was filtered with a smoothing kernel. Soft tissues are visible with similar contrast in both imaging modalities. The higher resolution obtained with the μCT device offers a more detailed insights in the regions of cartilage alterations and defects of the subchondral plate (Fig. 3).

In the next step the spatial resolution of the μCT scans could be improved by a factor of almost three by removing the skin, fat and muscles and extracting the tibia. As expected the formalin solution, where the tibia was stored in order to prevent it from drying out, made the identification of soft tissues more difficult. Nevertheless cartilage, menisci and ligaments could be recognized. The higher spatial resolution uncovered the demarcation between cartilage and menisci. The μCT data acquired in this step was used to choose the ROI for the extraction of the cylinders.

After the extraction of the cylindrical specimens the spatial resolution could be decresed to the micrometer level. As expected, the decrease of resolution in absorption based measurements did not offer better contrast within soft tissues (Fig. 5). It should still be highlighted that the laboratory absorption based μCT allowed the identification of ACL fibre bundles (Fig. 7). Along the demarcation of bone and cartilage an intermediate layer, associated with the mineralized cartilage zone, was clearly visible [16,17]. The tide mark line and calcified chondrocytes were identified. To the knowledge of the authors, these structures have so far not been visualized by a laboratory based tomographic device without the use of contrast agents [18].

All the absorption contrast data sets point out that X-ray phase contrast measurements are required for the visualization of soft tissues. To the best of our knowledge XGI was applied for the first time for tomographic

imaging of human knee tissues. One of the main questions here was the choice of the photon energy [7]. The relatively high energy chosen at the ESRF (section 3.4) led to an overall reasonable image contrast: bone and cartilage regions were visualized simultaneously. Nevertheless, due to the high energy, the cartilage morphology on the cellular level could not be revealed. The decrease of the energy at Diamond Light Source enabled a higher sensibility for cartilage tissue without giving the possibility to visualize the bone. The results shown in section 3.5 indicate that XGI is a competitive imaging technique compared to other X-ray phase contrast modalities like analyzer-based imaging (ABI) [19] or propagation-based PCI [17]. The main problem with the low energy measurements were the artefacts in the region of subchondral bone. In the next step these regions could be replaced by the absorption signal of the XGI, or even better by the nanotom® m data. All these different modalities (including the scattering signal) can be merged showing complimentary information [20]. This would allow showing the subchondral bone and the cartilage on the cellular level and reasonable contrast. Osteoarthritis research might highly benefit from an imaging modality that allows the analysis of cartilage tissue and subchondral bone simultaneously.

Following the rather qualitative approach of the present work, the question arises whether structural cartilage matrix properties can be depicted in a more quantitative manner. This would involve the segmentation of the chondrocyte lagunae within the tomographic images. If a simple threshold approach would not be successful a more sophisticated segmentation approach (e.g. Frangi's filter [21]) could be applied. This would allow investigation of cell density, orientation or shape [17]. This could help to understand the morphological differences between intact and osteoarthritic cartilage matrices. Furthermore, the combination using a joint histogram of μCT and selected histological slices could allow identifying anatomical structures, which can neither be extracted from one or the other modality on their own [22].

One of the main advantages of XGI is the potential use in laboratory μCT systems. Several current research projects use XGI in laboratory-based μCT scanners [23, 24]. Having shown the feasibility of the XGI technique for human joint tissue, this offers a great chance for future cartilage research such as cartilage tissue engineering [25].

ACKNOWLEDGMENTS

REFERENCES

[1] "http:www.wheelessonline.comortho/bone_remodeling,"

[2] Chen, H., Shoumura, S., Emura, S., and Bunai, Y., "Regional variations of vertebral trabecular bone microstructure with age and gender," *Osteoporos. Int.* **19**, 1473–1483 (2008).

[3] Stauber, M. and Müller, R., "Volumetric spatial decomposition of trabecular bone into rods and plates?A new method for local bone morphometry," *Int. Mater. Rev.* **38**, 474–484 (2006).

[4] Stauber, M., Rapillard, L., van Lenthe, G. H., Zysset, P., and Müller, R., "Importance of Individual Rods and Plates in the Assessment of Bone Quality and Their Contribution to Bone Stiffness," *J. Bone Miner. Res.* **21**, 586–595 (2006).

[5] Peyrin, F., Dong, P., Pacureanu, A., and Langer, M., "Micro- and nano-CT for the study of bone ultrastructure," *Curr. Osteoporos. Rep.* **12**, 465–474 (2014).

[6] Drews, S., Beckmann, F., Herzen, J., Brunke, O., Salmon, P., Friess, S., Laib, A., Koller, B., Hemberger, T., Müller-Gerbl, M., and Müller, B., "Comparative micro computed tomography study of a vertebral body," *Proc. SPIE* **7078**, 70780C (2008).

[7] Holme, M. N., Schulz, G., Deyhle, H., Weitkamp, T., Beckmann, F., Lobrinus, J. A., Rikhtegar, F., Kurtcuoglu, V., Zanette, I., Saxer, T., and Müller, B., "A complete estimate of the phylogenetic relationships in Ruminantia: a dated species-level supertree of the extant ruminants," *Nature Prot.* **9**, 1401–1415 (2014).

[8] Müller, B., Deyhle, H., Lang, S., Schulz, G., Bormann, T., Fierz, F., and Hieber, S., "Three-dimensional registration of tomography data for quantification in biomaterials science," *Int. J. Mater. Res.* **103**, 242–249 (2012).

[9] Müller-Gerbl, M., "Anatomy and biomechanics of the upper ankle joint," *Orthopade* **30**, 3–11 (2001).

[10] Weitkamp, T., David, C., Kottler, C., Bunk, O., and Pfeiffer, F., "Tomography with grating interferometers at low-brilliance sources," *Proc. SPIE* **6318**, 63180S (2006).

[11] Faris, G. W. and Byer, R. L., "Three-dimensional beam-deflection optical tomography of a supersonic jet," *Appl. Opt.* **27**, 5202–5212 (1988).

[12] Pfeiffer, F., Bunk, O., Kottler, C., and David, C., "Tomographic reconstruction of three-dimensional objects from hard X-ray differential phase contrast projection images," *Nucl. Instrum. Methods Phys. Res. Sect. A* **580**, 925–928 (2007).

[13] Andronache, A., von Siebenthal, M., Székely, G., and Cattin, P., "Non-rigid registration of multi-modal images using both mutual information and cross-correlation," *Med. Image Anal.* **12**, 3–15 (2008).

[14] Maes, F., Collignon, A., Vandermeulen, D., Marchal, G., and Suetens, P., "Multi-modality image registration by maximization of mutual information," *Proc. IEEE Math. Meth. in Biomed. Im. Anal.* , 14–22 (1996).

[15] Viola, P. and Wells, W. M., "Alignment by maximization of mutual information," *Proc. 5th Int. Conf. on Comp. Vis.* , 16–23 (1995).

[16] Buckwalter, J. and Mankin, H., "Articular cartilage, part I: tissue design and chondrocyte-matrix interactions," *J. Bone Joint Surg.* **79**, 600–611 (1997).

[17] Zehbe, R., Haibel, A., Riesemeier, H., Gross, U., Kirkpatrick, C. J., Schubert, H., and Brochhausen, C., "Going beyond histology. Synchrotron micro-computed tomography as a methodology for biological tissue characterization: from tissue morphology to individual cells," *J. R. Soc. Interface* **7**, 49–59 (2010).

[18] Li, X. F., Cai, X. R., Fan, F., Niu, H. J., Li, S. Y., Li, D. Y., Fan, Y. B., and Qin, Y. X., "Observation of sGAG content of human hip joint cartilage in different old age groups based on EPIC micro-CT," *Connect. Tissue Res.* **56**, 99–105 (2015).

[19] Coan, P., Bamberg, F., Diemoz, P. C., Bravin, A., Timpert, K., Mtzel, E., Raya, J. G., Adam-Neumair, S., Reiser, M. F., and Glaser, C., "Characterization of osteoarthritic and normal human patella cartilage by computed tomography X-ray phase-contrast imaging: a feasibility study," *Invest. Radiol.* **45**, 437–444 (2010).

[20] Schulz, G., Waschkies, C., Pfeiffer, F., Zanette, I., Weitkamp, T., David, C., and Müller, B., "Multimodal imaging of human cerebellum - merging X-ray phase microtomography, magnetic resonance microscopy and histology.," *Sci. Rep.* **2**, 826 (2012).

[21] Manniesing, R. and Niessen, W., "Multiscale vessel enhancing diffusion in CT angiography noise filtering," *Info. Proc. Med. Imag.* , 138–149 (2005).

[22] Stalder, A. K., Ilgenstein, B., Chicherova, N., Deyhle, H., Beckmann, F., Müller, B., and Hieber, S., "Combined use of micro computed tomography and histology to evaluate the regenerative capacity of bone grafting materials," *Int. Mater. Rev.* **105**, 679–691 (2014).

[23] Pfeiffer, F., Weitkamp, T., Bunk, O., and David, C., "Phase retrieval and differential phase-contrast imaging with low-brilliance X-ray sources," *Nature Phys.* **2**, 258–261 (2006).

[24] Khimchenko, A., Schulz, G., Deyhle, H., Hieber, S. E., Hasan, S., Bikis, C., Schulz, J., Costeur, L., and Müller, B., "Non-destructive phase contrast hard X-ray imaging to reveal the three-dimensional microstructure of soft and hard tissues," *Proc. SPIE* **9797**, 97970B (2016).

[25] Olubamiji, A. D., Izadifar, Z., and Chen, D. X., "Synchrotron imaging techniques for bone and cartilage tissue engineering: potential, current trends, and future directions," *Tissue Eng. Part B Rev.* **20**, 503–522 (2014).